

Communication

Sub-kHz Narrow-Linewidth Single-Longitudinal-Mode Thulium-Doped Fiber Laser Utilizing Triple-Coupler Ring-Based Compound-Cavity Filter

Biao Guan ¹, Fengping Yan ^{1,*}, Dandan Yang ¹, Qi Qin ¹ , Ting Li ¹, Chenhao Yu ¹, Xiangdong Wang ¹, Kazuo Kumamoto ²  and Yuping Suo ³¹ School of Electronic and Information Engineering, Beijing Jiaotong University, Beijing 100044, China² Department of Electronics, Information and Communication Engineering, Osaka Institute of Technology, Osaka 535-8585, Japan³ Shanxi Provincial People's Hospital, Shanxi Medical University, Taiyuan 030012, China

* Correspondence: fpyan@bjtu.edu.cn

Abstract: This paper proposes and demonstrates a single-longitudinal-mode thulium-doped fiber laser using a passive triple-coupler ring-based compound-cavity filter (TCR-CC) and a uniform fiber Bragg grating. For the first time, the TCR-CC filter is used to select a single mode from dense longitudinal modes. Experimental results show that laser in the wavelength of 1941.28 nm can maintain exceptional stability with an optical signal-to-noise ratio of 74.1 dB. The measured maximum wavelength drift and power fluctuation are 0.01 nm and 0.45 dB, respectively. Meanwhile, the measured linewidth of the laser is 910 Hz, and the relative intensity noise is below -125.82 dB/Hz above 2 MHz frequencies.

Keywords: single-longitudinal-mode; thulium-doped fiber laser; triple-coupler ring-based compound-cavity filter



Citation: Guan, B.; Yan, F.; Yang, D.; Qin, Q.; Li, T.; Yu, C.; Wang, X.; Kumamoto, K.; Suo, Y. Sub-kHz Narrow-Linewidth Single-Longitudinal-Mode Thulium-Doped Fiber Laser Utilizing Triple-Coupler Ring-Based Compound-Cavity Filter. *Photonics* **2023**, *10*, 209. <https://doi.org/10.3390/photonics10020209>

Received: 15 January 2023

Revised: 3 February 2023

Accepted: 6 February 2023

Published: 14 February 2023



Copyright: © 2023 by the authors. Licensee MDPI, Basel, Switzerland. This article is an open access article distributed under the terms and conditions of the Creative Commons Attribution (CC BY) license (<https://creativecommons.org/licenses/by/4.0/>).

1. Introduction

Narrow-linewidth single-longitudinal-mode (SLM) fiber lasers have been extensively explored owing to their advantages like long coherent length, which can be advantageously applied in various fields, including fiber sensing [1], Doppler LIDAR [2], coherent beam combination [3], gravitational-wave observation [4], and high precision optical measurement systems [5]. Several techniques have been reported so far to realize SLM fiber laser, including short-cavity distributed Bragg reflector (DBR) [6], distributed feedback (DFB) structure [7], Raman fiber laser [8], compound-ring cavity fiber laser [9], and optical self-injection feedback [10].

Despite their compactness and robustness in the SLM operation, DBR and DFB fiber lasers have some inherent structural limitations that prevent them from achieving wide tunability. SLM ring cavity fiber lasers are free from these limitations due to their flexibility in embedding various spectral filters. The ring lasers with long cavity lengths lead to narrow linewidth based on Schawlow-Townes theory [11] and the relaxation oscillation frequency peak shifts towards lower frequency. It is more susceptible to mode-hopping and multi-longitudinal mode oscillation due to densely spaced resonant modes in low frequency. To circumvent these drawbacks, numerous mode-selection mechanisms have been investigated. The unpumped active fibers based on saturable absorber (SA) can restrict the laser's longitudinal modes and strengthen the single-mode oscillation in a SA. Yin et al. demonstrated a stable SLM thulium-doped fiber laser (TDFL) using a SA as self-tracking narrow-band filter [12]. However, the approach caused a large amount of laser energy to be absorbed by SA, resulting in a large cavity loss. Narrow bandwidth filters are a crucial tool for SLM operation. Cheng et al. presented a simple and stable SLM fiber laser that

consists of an apodized uniform fiber Bragg grating (UFBG) and a high finesse FBG-based Fabry–Perot (F-P) etalon in the ring cavity [13]. The manufacturing process was strict due to ultra-narrow bandwidth of FBG. The compound-cavity composed of sub-ring cavity filters can expand longitudinal mode interval according to the vernier effect [14] resulting in a low production cost. Feng et al. used a four-wavelength-switchable erbium-doped fiber laser with a superimposed high-birefringence FBG and a dual-coupler ring-based compound-cavity filter to achieve SLM operation [15]. Furthermore, Cheng et al. proposed and demonstrated a six-wavelength SLM thulium-doped fiber laser, which was guaranteed by a novel passive dual-ring compound cavity composed of two symmetric 3×3 optical couplers [16]. Although some passive sub-ring resonators have been designed, developing more effective passive sub-ring resonators is still important for potential applications requiring extremely high stability and ultra-narrow linewidth. To further improve the output linewidth and stability performance, it is useful to use the compound-ring cavity filter with transmission spectrum owing to the narrow main resonance peak.

In this paper, a mode of analysis for a compound-ring cavity mode-selection mechanism is established. The evolution characteristics of the SLM operation is demonstrated based on theoretical analysis. Herein, a main ring cavity consists of a UFBG and a triple-coupler ring-based compound-cavity (TCR-CC) filter. A laser of 1941.28 nm with a 74.1 dB optical signal-to-noise ratio (OSNR) was obtained when the pump power was 2.1 W. The experimental results indicated that the laser exhibits exceptional spectral stability within one hour. Moreover, the radio frequency (RF) spectra with different ranges were given to verify the SLM operation. Finally, the relative intensity noise (RIN) of the proposed laser was -125.82 dB/Hz at frequencies above 2 MHz, and the linewidth was 910 Hz with an integration time of 0.001 s.

2. Experimental Setup and Principles

2.1. Experimental Configuration

The experimental setup of the proposed SLM TDFL utilizing a TCR-CC filter is shown in Figure 1a. A 3.5 m-long thulium-doped fiber (TDF, SM-TDF10P/130-HE, Coherent, Santa Clara, CA, USA) as an active media was pumped using a 793 nm pump (K793DA3RN-12.00W, BWT Beijing Ltd., Beijing, China) through a fiber combiner (FC, LightComm Technology, China). The peak cladding absorption of TDF at 793 nm is 3 dB/m, and it can offer sufficient gain to the fiber laser with high conversion efficiency. The core/cladding diameters of TDF and FC's output pigtails are both 10/130 μm .

To ensure a counterclockwise transmission of laser, a circulator was inserted between the optical coupler (OC_4) and FC. An optical spectrum analyzer (OSA, AQ6375B, Yokogawa, Japan) with a resolution of 0.05 nm and a sampling interval of 0.01 nm was used to measure 10% of laser power from the 10/90 OC. It can be connected to a photodetector (PD) that can convert light signals into electronic signals injected into the signal analyzer. The length of the main cavity L was 11.3 m, which provided an 18.4 MHz longitudinal-mode spacing according to $\Delta\nu = c/n_{\text{eff}}L$, where $c = 3 \times 10^8$ m/s is the speed of light in vacuum, and $n_{\text{eff}} = 1.4414$ is the refractive index of the fiber at 2 μm band. A TCR-CC filter made of two 2×2 couplers (OC_2, OC_3) and a 3×3 coupler (OC_1) is shown in Figure 1b. The UFBG was fabricated in a uniform phase mask (period $\Lambda = 1347.3$ nm), and a 248 nm KrF excimer laser. The transmission and reflection spectra of UFBG were detected by an amplified spontaneous emission (ASE), as shown in Figure 1c. The peak reflection wavelength is 1941.28 nm, the corresponding reflectivity is 75%, and the reflection bandwidth (RB) is 0.12 nm.

2.2. Principle of SLM Operating

The TCR-CC was injected in the ring cavity because the UFBG with a 3 dB bandwidth of 8.6 GHz was not narrow enough to directly produce a SLM laser. The TCR-CC filter, as shown in Figure 1b, was assembled by three OCs. We set $E_{in1}-E_{14}$ as the electric-field amplitudes of each light port, L_1-L_4 as the fiber lengths, κ_1 as the cross-coupling ratio, γ_1

and γ_2 as the insertion loss of the OCs, α as the fiber loss coefficient, δ as the fusion splicing loss, $\beta = 2\pi n_{eff} / \lambda$ as the light propagation constant, n_{eff} as the effective refractive index, and λ as the wavelength.

According to Mason’s rule [17], with the signal-flow graph in Figure 2, the lasing transmission at each node is given by:

$$\begin{cases} C_1 = \sqrt{1 - \gamma_1} / \sqrt{3} \\ Z_1 = \sqrt{1 - \gamma_1} e^{i2\pi/3} / \sqrt{3} \\ X_m = \sqrt{1 - \kappa_m} \sqrt{1 - \gamma_m} (m = 2, 3) \\ Y_m = i\sqrt{\kappa_m} \sqrt{1 - \gamma_m} (m = 2, 3) \\ T_n = \sqrt{1 - \delta} e^{(-\alpha + j\beta)L_1} (n = 1, 2, 3, 4) \end{cases} \quad (1)$$

The straight transmittance of the OC₁ is labeled as C₁ and the cross-coupling transmittance is labeled as Z₁. Different from the 3 × 3 coupler, the straight transmittance of the OC_m (m = 2, 3) is labeled as X_m and the cross-coupling transmittance is labeled as Y_m. The propagation gain of the fiber optical path is labeled as T_n. Considering the operation of the light, input power was set as E_{in1} = 1, E₂ = E₃ = E₈ = E₁₂ = 0, and the process of the laser can be written as:

$$\begin{cases} E_{in1} = 1 \\ E_4 = C_1 E_1 + Z_1 E_2 + Z_1 E_3 \\ E_5 = Z_1 E_1 + C_1 E_2 + Z_1 E_3 \\ E_6 = Z_1 E_1 + Z_1 E_2 + C_1 E_3 \\ E_7 = T_1 E_4 \\ E_9 = X_2 E_7 + Y_2 E_8 \\ E_{10} = Y_2 E_7 + X_2 E_8 \\ E_{11} = T_2 E_9 \\ E_{13} = X_3 E_{11} + Y_3 E_{12} \\ E_{14} = Y_3 E_{11} + X_3 E_{12} \\ E_2 = T_4 E_{14} \\ E_3 = T_3 E_{13} \end{cases} \quad (2)$$

The solution of E₁₀ can be calculated through the above equations and the transmission T of the TCR-CC filter can be written as:

$$T = \left(\frac{E_{out10}}{E_{in1}} \right) \cdot \left(\frac{E_{out10}}{E_{in1}} \right)^* \quad (3)$$

The transmission spectra of the TCR-CC filter were obtained by simulation, and the result is shown in Figure 3. The main cavity’s longitudinal mode spacing of 18.4 MHz is close to the effective 3 dB bandwidth of the TCR-CC filter, which ensures that only one longitudinal mode is dominant in the transmission band. Moreover, the TCR-CC filter’s effective free-spectral range (FSR) should be at least as wide as its 3 dB bandwidth. Based on the determined cavity length of Ring 1 and Ring 2, according to the above analysis, the influence of the coupling ratio κ on the TCR-CC filtering characteristics was simulated in detail, as shown in Figure 3. The used parameters were $\beta = 0.2$ dB/km, $\delta = 0.01$ dB, $\gamma_i (i = 1, 2, 3) = 0.09$ dB, $n_{eff} = 1.4414$, $L_1 = 0.7$ m, $L_2 = 0.7$ m, $L_3 = 0.7$ m, $L_4 = 0.73$ m. The coupling ratio of OC₁ is 1:1:1. For the TCR-CC filter, the transmission spectra were simulated for the values of the coupling ratio κ_3 of 0.1, 0.5, and 0.9, respectively, as shown in Figure 3a–c. The coupling ratio κ_2 was defined as 0.5. As can be seen, the transmission of the TCR-CC filter increased from 0.63 to 0.81, then dropped down to 0.63, while the FSR maintained the constant of 6.9 GHz determined by the ΔL of 3 cm. To obtain a high transmissivity of the proposed fiber laser, the ratio κ_3 was chosen as 0.5. Moreover, the influence of OC₂’s ratio can be seen in Figure 3d,e; the transmission of the filter with OC₂’s ratios of 0.1 and 0.9 was lower than that at the ratio of 0.5. Therefore, the ratio of OC₂ was set to 0.5. The main resonant peak of TCR-CC filter can be observed through partial enlarged view, as shown in Figure 3f. The 3 dB bandwidth of the main resonant peak was 18.5 MHz,

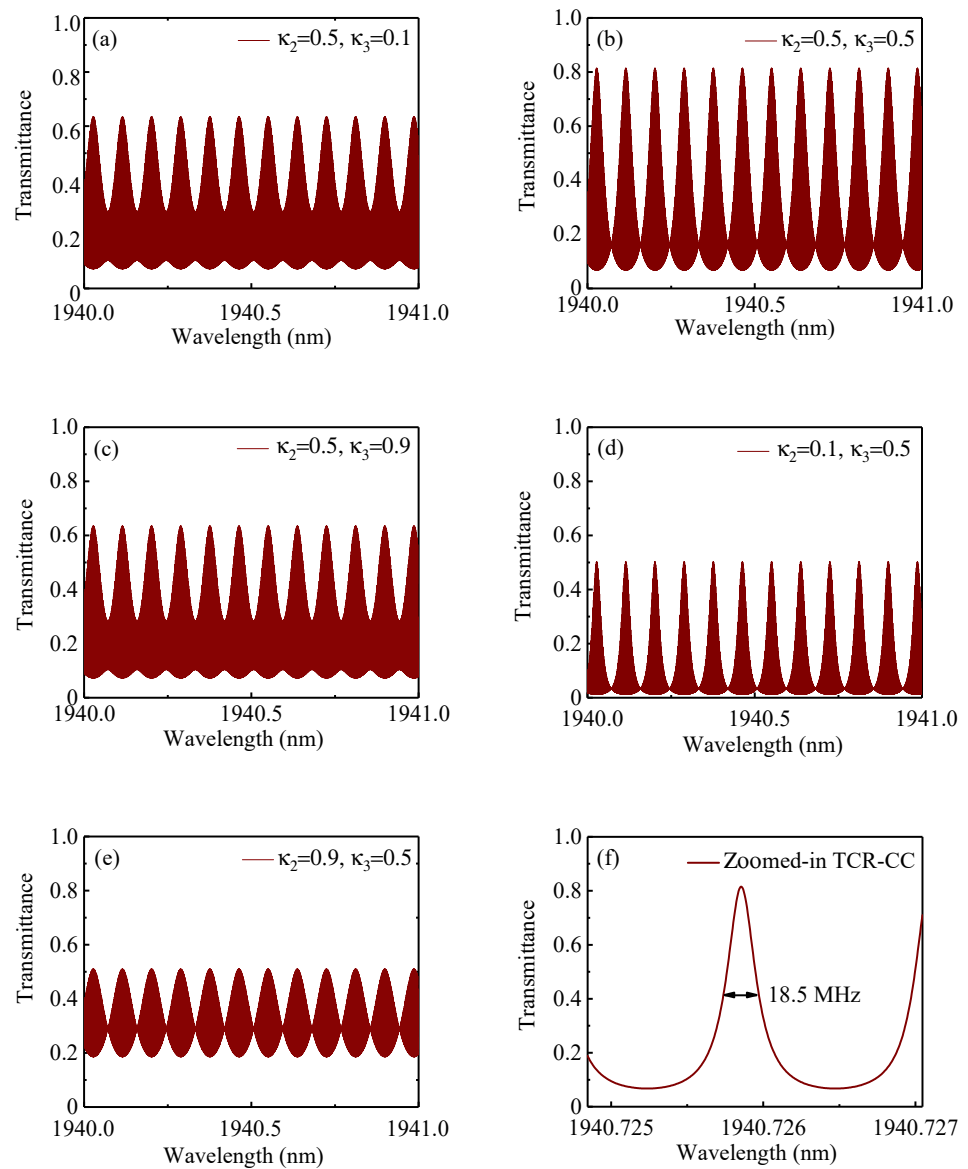


Figure 3. Simulated spectra of the proposed TDCR-CC filter (a–e) showing the influence of the ratio on the transmission performance. (f) The zoomed-in transmission spectrum of TCR-CC at main resonance peak.

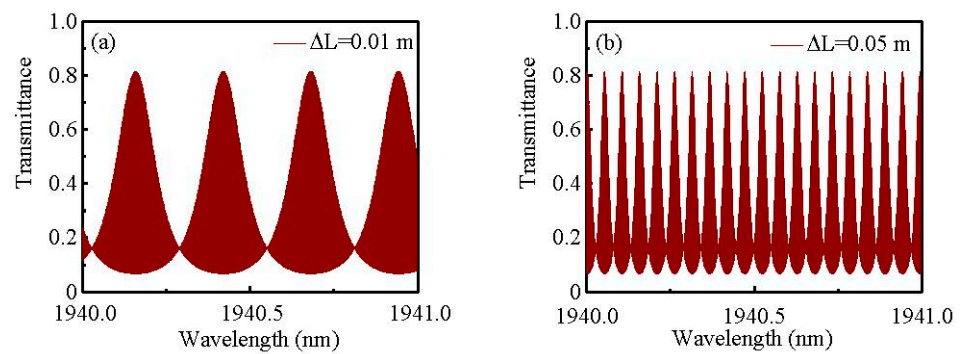


Figure 4. Simulated spectra of the proposed TCR-CC filter, with (a,b) showing the influence of sub-ring cavity length on the transmission performance.

3. Experimental Results

The optical spectrum of proposed TDFL with the pump power of 2.1 W was measured by OSA with a span of 10 nm. A sharp unimodal with an OSNR of more than 74.1 dB can be observed in Figure 5a. The lasing stability was demonstrated in the inset of Figure 5a, which was recorded for 60 min in 5 min intervals. Figure 5b shows the medium-term operating stability at a lasing wavelength of 1941.28 nm, which demonstrates that the laser operates with good wavelength stability, and the maximum wavelength fluctuation is 0.01 nm. The power fluctuation of 0.45 dB was produced by the pump source due to vibration caused by an internal device during heat radiation. Moreover, the thermal effects accumulated over a prolonged period of the laser operation can cause power fluctuation. The temperature change caused by the continuous operation of the pump will affect the refractive index of the optical fiber and cause wavelength fluctuation.

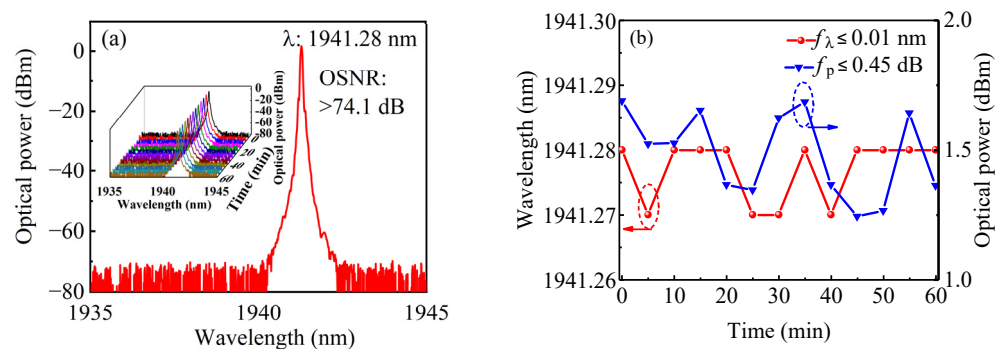


Figure 5. (a) Measured optical spectrum of proposed TDFL with pump power of 2.1 W. (b) Fluctuations of wavelength and power of 1941.28 nm.

The SLM property was detected by a 12.5 GHz PD and a 26.5 GHz signal analyzer (Keysight, N9020A) when the TDFL was operating at 2.1 W pump power. Figure 6a displays the RF spectrum with a resolution bandwidth (RBW) of 1 MHz and a span of 100 MHz. It can be noticed that this fiber laser operates in SLM status. A detailed drawing of signal analyzer results is shown in the inset of Figure 6a and the RF spectrum was continuously monitored for 60 min. As can be seen in Figure 6b,c, no beat frequency can be observed in the scanning range of 0–500 MHz and 0–1 GHz, indicating that the TDFL was operating at a stable SLM state. To further investigate the mode suppression property of TCR-CC structure, the TCR-CC filter was removed in the ring cavity and replaced with single-mode fiber of the same length. As can be seen in Figure 6d, the spacing of the main cavity's longitudinal mode is 18.4 MHz, which is consistent with the above-mentioned results. The comparison of different SLM states under two conditions indicated that the TCR-CC can constrain multi-longitudinal modes and the proposed laser combined with FBG and TCR-CC can operate in the SLM state.

One typical RIN spectrum was investigated for the TDFL by a system composed of a 12.5 GHz PD and an oscilloscope (Tektronix, DPO7104), as shown in Figure 7. Obviously, the RIN of the SLM TDFL was lower than -125.82 dB/Hz at frequencies over 2 MHz, and a range of 0–500 kHz was given in the inset of Figure 7. Theoretically, the RIN below -120 dB/Hz can satisfy the application requirements, such as an interferometric fiber sensing laser [18]. The relaxation oscillation frequencies peak of 52.5 kHz can be observed in the inset, which was mainly influenced by the cavity length, pump power, cavity loss, mechanical vibration, and thermal disturbance [19].

The linewidth of the fiber laser was measured using the unbalanced Michelson interferometer involving a 3×3 coupler, two Faraday rotation mirrors, and a 50 m single-mode fiber [20]. The linewidth was calculated through laser phase noise demodulation based on the β -separation linewidth method under different integration times, and the results are reported in Figure 8 [21–23]. The laser linewidth at different integration times (0.001, 0.005, 0.01, 0.05, 0.1, 0.5, and 1 s) were 0.91, 18.09, 20.49, 24.67, 30.37, 87.27, and 278.91 kHz,

respectively. As can be seen, the linewidth was 910 Hz at the minimum measurement time, which is the intrinsic linewidth of the laser. Meanwhile, the measured linewidths gradually expand as the integration time increases. These increasing values were primarily a result of technical noise brought on by environmental vibrations and low-frequency signal interference during the experiment. In addition, the linewidth was affected by the thermal effect accumulated by the cladding pump due to prolonged operation.

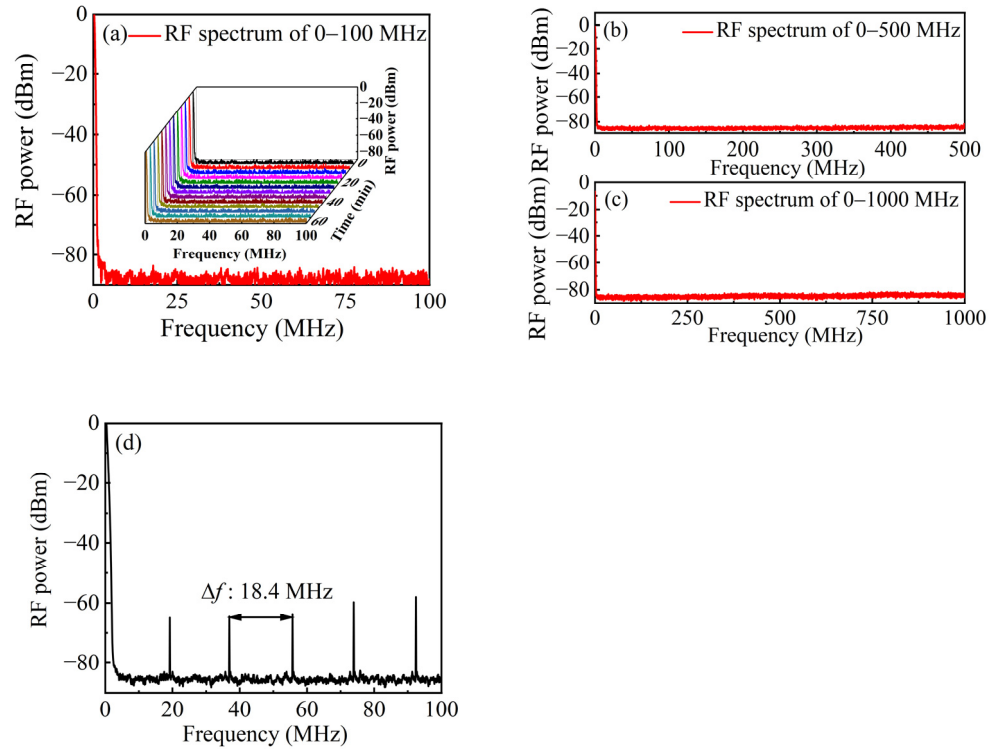


Figure 6. RF spectrum measured by signal analyzer in the range of (a) 0–100 MHz with a RBW of 500 kHz, (b) 0–500 MHz, (c) 0–1 GHz. (d) The spectrum of the main cavity without the TCR-CC filter.

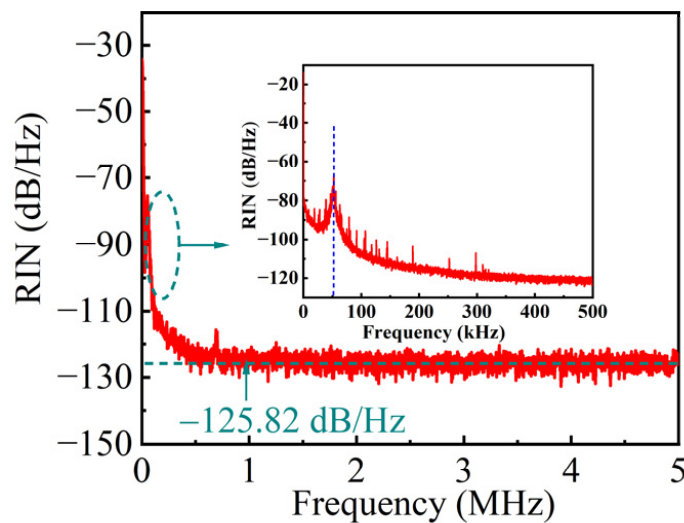


Figure 7. RIN spectrum of the laser with a frequency range of 0–5 MHz with a 10 kHz RBW, and inset shows the same measurement in 0–500 kHz using RBW of 100 Hz.

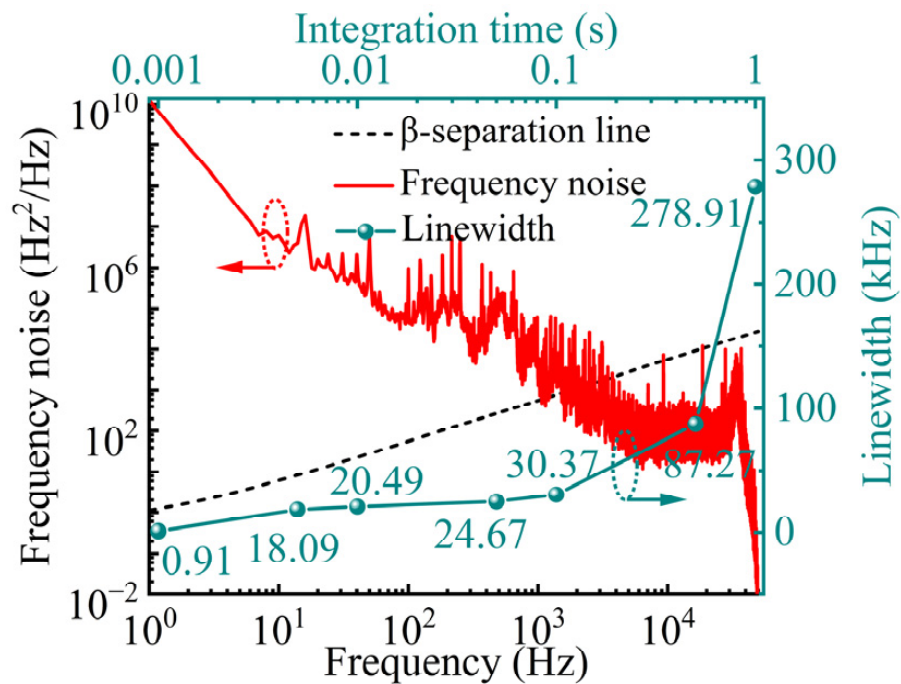


Figure 8. Frequency noise power spectral density of the proposed laser and linewidth at different integration times.

Moreover, the proposed fiber laser is compared with some of the previously reported TDFLs with different technique, as shown in Table 1. The maximal power fluctuation in the TDFL proposed in this paper is 0.45 dB, which is lower than in the report [24]. The OSNR is higher than that in the previous reports [24–27], and the exceptional OSNR is obtained. In addition, compared with fiber lasers using other technique, the linewidth of the proposed TDFL can reach a narrow value. It can be seen from the comparison results that the laser proposed in this paper has the advantages of high OSNR and high stability.

Table 1. Wavelength, Maximal power, OSNR comparison of SLM TDFL based on different techniques.

Technique	Wavelength /nm	Maximal Power Fluctuation	OSNR	Linewidth	Reference
Self-injection + SA	1923.44	0.7 dB	25 dB	<9.1 MHz	[24]
DBR	1950	NA	58 dB	6.95 kHz	[25]
FBG + SA	1950.06	NA	68 dB	6.76 kHz	[26]
SA	1957.24	NA	60 dB	20 kHz	[12]
Micro resonator	1978.6	NA	55 dB	15.1 kHz	[27]
This work	1941.28	0.45 dB	74.1 dB	910 Hz	

The relationship between laser output power and pump power was measured by a power meter (Laser point). As can be seen in Figure 9, the laser began to lase with an output power of 0.24 mW when the pump power was 2.05 W, and the output power increased with the increasing pump power. Three measurements of the output power were taken for each pump power, and the average power was then computed. When the pump power was 6.5 W, the average output power was 75.92 mW and the slope of the laser was about 1.76%. The reason of low output power is the mode field mismatch loss caused by the size mismatch during the fusion splicing between TDF and SMF.

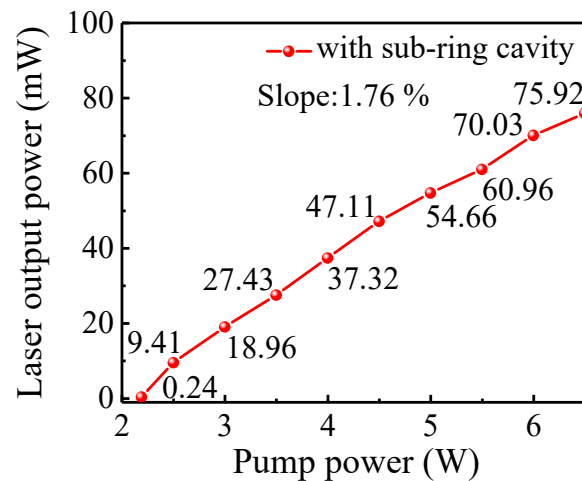


Figure 9. Output power variations of the laser with different pump powers.

4. Conclusions

A SLM TDFL centered at 1941.28 nm with an OSNR as high as 74.1 dB was constructed. The stable SLM operation was obtained by combining a UFBG and a TCR-CC filter. The design and characterization of the TCR-CC filter were presented in detail. The fluctuations of the wavelength and corresponding output power were less than 0.01 nm and 0.47 dB, respectively. Experimental results measured by the signal analyzer revealed the SLM characteristics. The RIN of the proposed laser was measured to be under -125.82 dB/Hz with frequencies above 2 MHz. Based on the β -separation line method, the linewidth of less than 910 Hz was calculated by the frequency noise power spectral density under different integration times. The output power increased up to 75.92 mW when the pump power was fixed at 6.5 W with a slope efficiency of 1.76%. The proposed TDFL has a great potential in free-space optical communication.

Author Contributions: Conceptualization, B.G.; methodology, B.G. and F.Y.; software, D.Y.; validation, Q.Q. and T.L.; resources, B.G., C.Y. and X.W.; data curation, D.Y., Y.S. and K.K.; writing—original draft preparation, C.Y. and X.W.; writing—review and editing, B.G., D.Y. and Q.Q.; supervision, B.G. and T.L.; project administration, B.G. All authors have read and agreed to the published version of the manuscript.

Funding: This research was supported by the Fundamental Research Funds for the Central Universities (No. 2022JBCG005), National Natural Science Foundation of China (No. 61827818, 61975105).

Institutional Review Board Statement: Not applicable.

Informed Consent Statement: Not applicable.

Data Availability Statement: The data presented in this study may be available from the corresponding author upon reasonable request.

Conflicts of Interest: The authors declare no conflict of interest.

References

- Zheng, H.; Zhang, J.; Guo, N.; Zhu, T. Distributed Optical Fiber Sensor for Dynamic Measurement. *J. Light. Technol.* **2021**, *39*, 3801–3811. [[CrossRef](#)]
- Henderson, S.W.; Hale, C.P.; Hannon, S.M.; Magee, J.R.; Bruns, D.L.; Yuen, E.H. Coherent Laser Radar at 2 pm Using Solid-state Lasers. *IEEE Trans. Geosci. Remote Sens.* **1993**, *31*, 4–15. [[CrossRef](#)]
- Yu, C.X.; Augst, S.J.; Redmond, S.M.; Goldizen, K.C.; Murphy, D.V.; Sanchez, A.; Fan, T.Y. Coherent combining of a 4 kW, eight-element fiber amplifier array. *Opt. Lett.* **2011**, *36*, 2686–2688. [[CrossRef](#)]
- Kwee, P.; Bogan, C.; Danzmann, K.; Frede, M.; Kim, H.; King, P.; Pöld, J.; Puncken, O.; Savage, R.L.; Seifert, F.; et al. Stabilized high-power laser system for the gravitational wave detector advanced LIGO. *Opt. Express* **2012**, *20*, 10617–10634. [[CrossRef](#)] [[PubMed](#)]

5. Passy, R.; Gisin, N.; von der Weid, J.P.; Gilgen, H.H. Experimental and Theoretical Investigations of Coherent OFDR with Semiconductor Laser Sources. *J. Light. Technol.* **1994**, *12*, 1622–1630. [[CrossRef](#)]
6. Yang, Q.; Xu, S.H.; Li, C.; Yang, C.S.; Feng, Z.M.; Xiao, Y.; Huang, X.; Yang, Z.M. A Single-Frequency Linearly Polarized Fiber Laser Using a Newly Developed Heavily Tm³⁺-Doped Germanate Glass Fiber at 1.95 μm . *Chin. Phys. Lett.* **2015**, *32*, 0942061-4. [[CrossRef](#)]
7. Walasik, W.; Traore, D.; Amavigan, A.; Tench, R.E.; Delavaux, J.M.; Pinsard, E. 2- μm Narrow Linewidth All-Fiber DFB Fiber Bragg Grating Lasers for Ho- and Tm-Doped Fiber-Amplifier Applications. *J. Light. Technol.* **2021**, *39*, 5096–5102. [[CrossRef](#)]
8. Loranger, S.; Karpov, V.; Schinn, G.W.; Kashyap, R. Single-frequency low-threshold linearly polarized DFB Raman fiber lasers. *Opt. Lett.* **2017**, *42*, 3864–3867. [[CrossRef](#)]
9. Feng, T.; Wang, M.; Wang, X.; Yan, F.; Suo, Y.; Yao, X.S. Switchable 0.612-nm-Spaced Dual-Wavelength Fiber Laser with Sub-kHz Linewidth, Ultra-High OSNR, Ultra-Low RIN, and Orthogonal Polarization Outputs. *J. Light. Technol.* **2019**, *37*, 3173–3182. [[CrossRef](#)]
10. Yeh, C.H.; Wang, B.Y.; Hsu, W.H.; You, W.Y.; Chen, J.R.; Chow, C.W.; Chen, J.H. Stable and selectable erbium multiple-ring laser with self-injection loop. *Opt. Laser Technol.* **2021**, *141*, 107106. [[CrossRef](#)]
11. Yariv, A.; Vahala, K. On the High Power Limit of the Laser Linewidth. *IEEE J. Quantum Electron.* **1983**, *19*, 889–890. [[CrossRef](#)]
12. Yin, T.; Song, Y.; Jiang, X.; Chen, F.; He, S. 400 mW narrow linewidth single-frequency fiber ring cavity laser in 2 μm wave-band. *Opt. Express* **2019**, *27*. [[CrossRef](#)]
13. Cheng, X.P.; Tse, C.H.; Zhou, J.L.; Tang, M.; Tan, W.C.; Wu, R.F.; Zhang, J. Single-Longitudinal-Mode Erbium-Doped Fiber Ring Laser Based on High Finesse Fiber Bragg Grating Fabry–Pérot Etalon. *IEEE Photonics Technol. Lett.* **2008**, *20*, 976–978. [[CrossRef](#)]
14. Lemieux, J.F.; Latrasse, C.; Tetu, M. 100 GHz frequency step-tunable hybrid laser based on a vernier effect between a Fabry-Perot cavity and a sampled fiber Bragg grating. *Adv. Semicond. Lasers* **1999**, *31*, 186–188.
15. Feng, T.; Jiang, M.; Wei, D.; Zhang, L.; Yan, F.; Wu, S.; Yao, X.S. Four-wavelength-switchable SLM fiber laser with sub-kHz linewidth using superimposed high-birefringence FBG and dual-coupler ring based compound-cavity filter. *Opt. Express* **2019**, *27*, 36662–36679. [[CrossRef](#)] [[PubMed](#)]
16. Cheng, D.; Yan, F.; Feng, T.; Zhang, L.; Han, W.; Qin, Q.; Li, T.; Bai, Z.; Yang, D.; Guo, Y.; et al. Six-Wavelength-Switchable SLM Thulium-Doped Fiber Laser Enabled by Sampled FBGs and 3×3 Coupler Based Dual-Ring Compound Cavity Filter. *IEEE Photonics J.* **2022**, *14*, 1–8. [[CrossRef](#)]
17. Mason, S.J. Feedback theory-further properties of signal flow graphs. *Proc. IRE* **1953**, *44*, 920–926. [[CrossRef](#)]
18. Cranch, G.A. Frequency noise reduction in erbium-doped fiber distributed-feedback lasers by electronic feedback. *Opt. Lett.* **2002**, *27*, 1114–1116. [[CrossRef](#)]
19. Tan, T.; Yang, C.; Wang, W.; Wang, Y.; Zhao, Q.; Guan, X.; Peng, M.; Gan, J.; Yang, Z.; Xu, S. Ultralow-intensity-noise single-frequency fiber-based laser at 780 nm. *Appl. Phys. Express* **2020**, *13*, 022002. [[CrossRef](#)]
20. Cheng, D.; Yan, F.; Feng, T.; Han, W.; Zhang, L.; Qin, Q.; Li, T.; Bai, Z.; Yang, D.; Guo, Y.; et al. Five-Wavelength-Switchable Single-Longitudinal-Mode Thulium-Doped Fiber Laser Based on a Passive Cascaded Triple-Ring Cavity Filter. *IEEE Photonics J.* **2022**, *14*, 1–8. [[CrossRef](#)]
21. Domenico, G.D.; Schilt, S.; Thomann, P. Simple approach to the relation between laser frequency noise and laser line shape. *Appl. Opt.* **2010**, *49*, 4801–4807. [[CrossRef](#)]
22. Xu, D.; Yang, F.; Chen, D.; Wei, F.; Cai, H.; Fang, Z.; Qu, R. Laser phase and frequency noise measurement by Michelson interferometer composed of a 3×3 optical fiber coupler. *Opt. Express* **2015**, *23*, 22386–22393. [[CrossRef](#)]
23. Zhang, L.; Yan, F.; Feng, T.; Han, W.; Guan, B.; Qin, Q.; Guo, Y.; Wang, W.; Bai, Z.; Zhou, H.; et al. Six-wavelength-switchable narrow-linewidth thulium-doped fiber laser with polarization-maintaining sampled fiber Bragg grating. *Opt. Laser Technol.* **2021**, *136*, 106788. [[CrossRef](#)]
24. Yang, W.; Lu, P.; Wang, S.; Liu, D.; Zhang, J.; Chen, E.; Liu, J. A Novel Switchable and Tunable Dual-Wavelength Single-Longitudinal-Mode Fiber Laser at 2 μm . *IEEE Photonics Technol. Lett.* **2016**, *28*, 1161–1164. [[CrossRef](#)]
25. Guan, X.; Yang, C.; Gu, Q.; Wang, W.; Tan, T.; Zhao, Q.; Lin, W.; Wei, X.; Yang, Z.; Xu, S. 55 W kilohertz-linewidth core-and in-band-pumped linearly polarized single-frequency fiber laser at 1950 nm. *Opt. Lett.* **2020**, *45*, 2343–2346. [[CrossRef](#)]
26. He, X.; Xu, S.; Li, C.; Yang, C.; Yang, Q.; Mo, S.; Chen, D.; Yang, Z. 1.95 μm kHz-linewidth single-frequency fiber laser using self-developed heavily Tm³⁺-doped germanate glass fiber. *Opt. Express* **2013**, *21*, 20800–20805. [[CrossRef](#)]
27. Zhang, J.N.; Yao, W.C.; Wang, H.T.; Zhou, W.; Wu, X.; Shen, D.Y. A Watt-Level Single-Frequency Fiber Laser at 2 μm Using a Silica Prolate Microresonator. *IEEE Photonics Technol. Lett.* **2019**, *31*, 1241–1244. [[CrossRef](#)]

Disclaimer/Publisher’s Note: The statements, opinions and data contained in all publications are solely those of the individual author(s) and contributor(s) and not of MDPI and/or the editor(s). MDPI and/or the editor(s) disclaim responsibility for any injury to people or property resulting from any ideas, methods, instructions or products referred to in the content.